OPEN ACCESS
Journal of Innovative Optical Health Sciences
Vol. 16, No. 2 (2023) 2230010 (17 pages)

DOI: 10.1142/S1793545822300105

World Scientific
www.worldscientific.com

Stimulated Raman scattering microscopy on biological cellular machinery

Jing Huang* and Minbiao Ji*,†,‡
*State Key Laboratory of Surface Physics and Department of Physics
Human Phenome Institute
Academy for Engineering and Technology
Key Laboratory of Micro- and Nano-Photonic Structures (Ministry of Education)
Fudan University, Shanghai 200433, P. R. China
†Yiwu Research Institute, Fudan University, Chengbei Road
Yiwu, Zhejiang 322000, P. R. China
‡minbiaoj@fudan.edu.cn

Received 30 July 2022
Accepted 24 August 2022
Published 30 September 2022

Benefiting from the developments of advanced optical microscopy techniques, the mysteries of biological functions at the cellular and subcellular levels have been continuously revealed. Stimulated Raman scattering (SRS) microscopy is a rapidly growing technique that has attracted broad attentions and become a powerful tool for biology and biomedicine, largely thanks to its chemical specificity, high sensitivity and fast image speed. This review paper introduces the principles of SRS, discusses the technical developments and implementations of SRS microscopy, then highlights and summarizes its applications on biological cellular machinery and finally shares our visions of potential breakthroughs in the future.

Keywords: Nonlinear optical microscopy; vibrational spectral imaging; coherent Raman scattering; biological cells.

1. Introduction

After the discovery of cell via a home-built optical microscope by Hooke in 1665,[1] the unseen mystery of microscopic world has been uncovered. Since then, cell as the basic unit for a living organism has greatly extended our understandings of biology, especially after the foundation of the cell theory.[2–4] Meanwhile, the symbiotic optical microscopy has been improved significantly. Historically, the visualization of specimen via Hooke's microscope was simple with two lenses but accompanied by non-negligible aberration. One eventful advance to correct aberration was promoted by Lister in 1830 by developing the achromatic objective.[5] Later, modern optical microscope with spatial resolution down to 0.2 μm was manufactured by Carl Zeiss, Ernst

‡Corresponding author.

Abbe and Otto Schott in 1857 with the advent of "Apochromat".[6] Notably, Abbe was the first to theoretically advance microscopy.[7] To enhance the image contrast, different microscopies were developed independently, e.g., polarized light microscopy, phase contrast microscopy, differential interference contrast microscopy and so on. A milestone for modern biological investigation was the invention of optical fluorescence microscopy,[8] especially after the discovery of dichromatic beam-splitting plate and the foundation of immunofluorescence by Coons and Kaplan in 1950.[9] Motivated by the need to image thick specimen nondestructively, confocal microscopy was introduced by Minsky in 1957.[10] Actually, the ultimate goal for microscopists and biologists is to realize "live imaging" noninvasively. Even though modern fluorescence microscopy can solve many issues on life science thanks to its high specificity and sensitivity with the help of fluorescent probes, external labeling is an inevitable disadvantage of this technique. After the advent of laser, the concomitant nonlinear optical microscopy (NLOM) can avoid external labeling while showing unprecedented capability for high-spatial-resolution imaging.[11,12] NLOM deciphers the nonlinearity between the laser intensity and the irradiated specimen, thus only occurs in a confined region in the focal volume.

Among various NLOMs, coherent Raman scattering (CRS) microscopy stands out due to its excellent chemical specificity and high imaging speed.[13–15] As a nonlinear Raman technique, CRS employs intrinsic molecular vibrational fingerprints of the investigated targets as imaging contrast and enhances the weak spontaneous Raman signal by several orders of magnitudes.[13,16,17] CRS microscopy is often considered as a spectral imaging modality. Compared with another vibrational spectral imaging technique for biomolecular analysis — infrared (IR) microscopy,[18–22] CRS microscopy has several advantages: first, CRS avoids water interference, which is critical for living systems; second, CRS offers higher spatial resolution at submicrometer scale with the use of visible/near-infrared wavelength, allowing chemical imaging of single cells.[23] Generally speaking, CRS microscopy includes coherent anti-Stokes Raman scattering (CARS) microscopy and stimulated Raman scattering (SRS) microscopy, with distinct nonlinear optical properties. CARS was first reported by Duncan *et al.* in 1982[24] and has attracted worldwide attention after the improvement by Xie and coworkers in 1999.[25] Despite its gradual developments during the last two decades, CARS has three major limitations: nonresonant background issue, spectral distortion relative to spontaneous Raman spectra and nonlinear relationship between CARS signal and molecular concentration. To overcome the aforementioned shortcomings of CARS, megahertz (MHz)-rate modulated SRS was exploited in Xie's lab 10 years after their implementation of CARS.[26] Similar idea of SRS microscopy was also proposed by another two groups independently nearly at the same time in 2009.[27,28] Over the past 10 years, many efforts have been contributed to burgeon the blossoming of SRS, including, but not limited to, technical improvements (e.g., sensitivity,[29–34] speed,[35–43] multi-/super-multiplex capability,[44–49] spatial resolution,[50–60] specificity[61–65] and apparatus miniaturization[66,67]), biomedical applications (label-free tissue histopathology,[68–76] biological metabolism,[61,77–82] neurodegenerative diseases,[83,84] microbiology[37,85–90] and pharmacology[91–97]) and material sciences applications.[98–103]

SRS microscopy has shown unique capabilities for imaging endogenous biochemical components in biological systems, especially for single cells at micrometer scale. Living cells are essential units playing vital roles and presenting high heterogeneity on their internal structures, as well as external microenvironments. The better characterization of cellular systems will undoubtedly deepen our knowledge in the field. In this review, we have focused on and summarized the SRS microscopy studies of biological cells.

2. Mechanisms of Spontaneous and Stimulated Raman Scattering

2.1. *Spontaneous Raman scattering*

Raman scattering was first reported by Raman and Krishnan in 1928,[104] in which the inelastic interactions between incident photons and target molecular vibrations were probed [Fig. 1(a)]. Raman effect can be understood by an induced molecular polarization $\mu(t)$ which occurs through the interaction between an incident field $\mathbf{E}_{\text{in}}(t) = \mathbf{E}_0 \cos(\omega_0 t)$ and a molecule with varied polarizability $\alpha(q)$.[105–107] $\alpha(q)$ depends on its molecular coordinate q. The

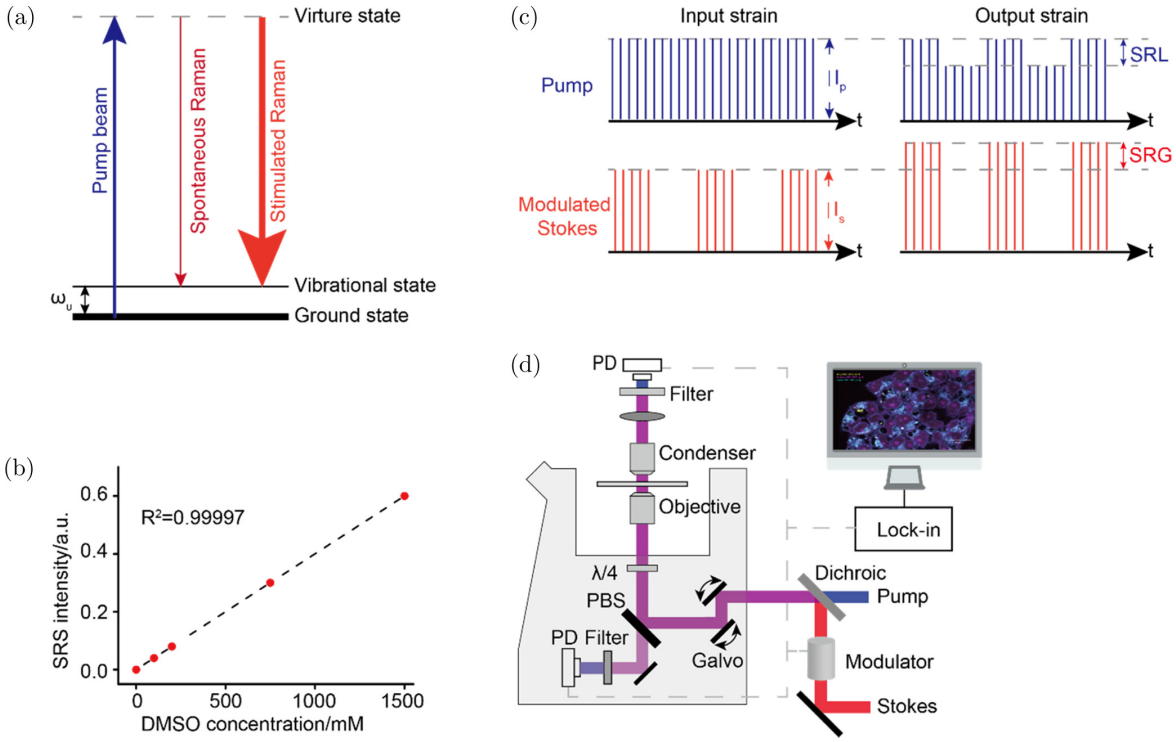

Note: PD: Photodiode and PBS: polarization beam splitter.

Fig. 1. Principle of SRS microscopy. (a) Energy diagram for SRS. (b) Linear dependence of SRL on concentrations of DMSO at 2915 cm^{-1}. (c) Detection schemes for SRL and SRG, Stokes is modulated at MHz. (d) Implementation of SRL microscope with both forward and EPI detection.

polarizability is typically expanded into Taylor series near the equilibrium position,

$$\alpha(q) = \alpha_0 + \left(\frac{\partial \alpha}{\partial q}\right)\Big|_{q=0} q(t) + \cdots . \tag{1}$$

The nuclear oscillation at resonant frequency ω_R can be approximated by a harmonic oscillation, resulting in

$$q(t) = q_0 \cos(\omega_R t). \tag{2}$$

Thus, the yielded induced molecular polarization is delineated as

$$\begin{aligned}\mu(t) &= \alpha(q)\mathbf{E}_{\text{in}}(t) \\ &= \alpha_0 \mathbf{E}_0 \cos(\omega_0 t) + \frac{1}{2}\left(\frac{\partial \alpha}{\partial q}\right)\Big|_{q=0} \\ &\quad \times q_0 \mathbf{E}_0 \cos(\omega_0 - \omega_R)t \\ &\quad + \frac{1}{2}\left(\frac{\partial \alpha}{\partial q}\right)\Big|_{q=0} q_0 \mathbf{E}_0 \cos(\omega_0 + \omega_R)t. \end{aligned} \tag{3}$$

From the above description, the induced polarization plays a role as the source of scattered radiation, resulting in three different frequencies: the same frequency ω_0 as the incident field known as elastic Rayleigh scattering, the difference frequency $\omega_0 - \omega_R$ named as Stokes and the sum frequency $\omega_0 + \omega_R$ called anti-Stokes, and the latter two with new frequencies result in inelastic Raman scattering. It is clear that "Raman-active" modes occur only when $(\frac{\partial \alpha}{\partial q})_0 \neq 0$. According to Boltzmann distribution, Stokes scattering is much stronger than anti-Stokes scattering. Notably, at room temperature, the scattered Stokes Raman intensity can be expressed as

$$I_{\text{Stokes}} = \text{constant} \times N I_0 (\omega_0 - \omega_R)^4 \left[\left(\frac{\partial \alpha}{\partial q}\right)\Big|_{q=0}\right]^2, \tag{4}$$

where "constant" denotes a constant value, N indicates the number of molecules and I_0 specifies the incident light intensity.[106,108]

2.2. *Stimulated Raman scattering*

Even though hitherto spontaneous Raman scattering is a common analytical technique for biomedical applications,[20,107,109,110] it usually occurs approximately once in 10^7 photon–molecule interactions.[107]

Such weak inherent signal cannot meet the need of high-speed biological imaging. One modality to overcome the low-signal limitation is to utilize nonlinear coherent Raman scattering effect, such as CARS and SRS. For CRS to occur, two beams coincide on the molecules, one supplied as the pump beam ω_p, and the other is the Stokes beam ω_S. In the presence of two incoming lasers, the nuclear displacement can be modeled as a damped harmonic oscillation driven by the beat of the pump and Stokes waves. When the beat frequency $\Omega = \omega_p - \omega_S$ resonates with the target molecular vibrational mode ω_R, the Raman signal will be coherently amplified.[16,17,105,111] In this paper, we focus on the nascent SRS microscopy, while CARS microscopy can be referred to in published reviews.[112–115]

In SRS, the total incident field is

$$\mathbf{E}_{\text{in}}(t) = \mathbf{E}_p(t) + \mathbf{E}_S(t), \tag{5}$$

and the total induced polarization is given by

$$\mathbf{p}(t) = N\alpha(q)\mathbf{E}_{\text{in}}(t) = N\left[\alpha_0 + \left(\frac{\partial\alpha}{\partial q}\right)\Big|_{q=0} q(t)\right] \times \{\mathbf{E}_p(t) + \mathbf{E}_S(t)\}. \tag{6}$$

The total induced polarization includes four distinct components: coherent Stokes Raman: $\omega_{\text{CS}} = 2\omega_S - \omega_p$, coherent anti-Stokes Raman: $\omega_{\text{AS}} = 2\omega_p - \omega_S$, stimulated Raman loss (SRL): $\omega_{\text{SRL}} = \omega_p$ and stimulated Raman gain (SRG): $\omega_{\text{SRG}} = \omega_S$. Thereby, the intensity of the pump beam I_p experiences a loss ΔI_p, and the intensity of the Stokes beam I_S experiences a gain ΔI_S. Hence, SRS signal is detected as a relative intensity change of the incident laser [$\frac{\Delta I}{I} \sim 10^{-3}$–$10^{-7}$, see Fig. 1(b)].[116] For example, the induced polarization at ω_{SRL} is given by

$$\mathbf{p}(\omega_{\text{SRL}}) = 6\varepsilon_0\chi_R^{(3)}(\Omega)\mathbf{E}_p(t)|\mathbf{E}_S(t)|^2, \tag{7}$$

where ε_0 is the vacuum permittivity, and $\chi_R^{(3)}$ is the third-order nonlinear susceptibility, which is expressed as

$$\chi_R^{(3)}(\Omega) = \frac{N}{6m\varepsilon_0}\left[\left(\frac{\partial\alpha}{\partial q}\right)\Big|_{q=0}\right]^2 \frac{1}{\omega_R^2 - \Omega^2 - 2i\Omega\gamma}, \tag{8}$$

where m denotes the reduced mass of the nuclear oscillator, γ is the damping constant of the damped harmonic oscillator.

The intensity of SRL is given by

$$\begin{aligned} S_{\text{SRL}} &\propto -N|\mathbf{E}_p(t)|^2|\mathbf{E}_S(t)|^2\mathbf{Im}\{\chi_R^{(3)}(\Omega)\} \\ &\propto -N\sigma_{\text{Raman}}I_pI_S, \end{aligned} \tag{9}$$

where σ_{Raman} represents the Raman cross-section. From Eq. (9), it is obvious that SRS intensity is linearly dependent on molecular concentration [Fig. 1(c)], which enables SRS to be a powerful tool for quantitative chemical analysis.

3. SRS Microscope Implementation

Figure 1(d) shows a typical SRS configuration with SRL detection. A dual-output pulsed OPO laser serves as the source, often the pump pulse is tunable (690–1300 nm) whereas the Stokes pulse at 1040 nm is modulated at MHz either via an electro-optic modulator (EOM) or via an acousto-optic modulator (AOM). The two pulses coincide temporally and spatially before guiding into a laser scanning microscope. Then the transmitted pump pulse is detected by a large-area silicon photodiode (PD) after filtering out the Stokes pulse. The output of PD detector is directed to a lock-in amplifier (LIA) for SRL signal demodulation. Actually, one can modulate the pump pulse then detect and demodulate SRG, but practically SRL detection is more favored than SRG detection since silicon PD responses weakly at the Stokes wavelengths (1040 nm or 1064 nm). The determination of studied vibrational Raman shift can be realized in many ways, e.g., by the tuning of a narrowband picosecond (ps) laser, or alternatively using spectral focusing approach for femtosecond (fs) pulses.

4. Technical Developments

4.1. *Imaging speed*

SRS enhances Raman signal by a factor of $\sim 10^3$–10^5,[116,117] making the imaging of live cells in second time scale possible. A typical acquisition time for SRS imaging with 2-μs pixel dwell time for a field of view with 512×512 pixels is about 1 s. With more advanced LIA and resonant galvanometer mirror, video-rate SRS imaging has been reported with 30–110 frames per second.[35–37] One advantage of SRS microscopy is the chemical mapping capability, which requires SRS spectral imaging within the target Raman frequency range.

Many efforts have been made to speed up multicolor/hyperspectral SRS microscopy, including sequential and parallel schemes [Fig. 2(a)]. Sequential wavelength tuning can be realized by wavelength sweeping on two synchronized narrowband picosecond lasers,[118,119] pulse shaping on a broadband femtosecond laser[120,121] or spectral focusing method on two broadband femtosecond lasers.[122–125] Sequential tuning modalities often demand simple instrumentation but take quite a long time. Among them, spectral focusing is getting more attention since it is relatively faster and more reproducible, the broadband femtosecond pump and Stokes pulses are chirped into picosecond by grating stretchers or glass rods, the two stretched pulses are time-dependent therefore the vibrational transitions can be chosen by changing the temporal "delay" between the two chirped pulses. A resonant mirror can rapidly adjust the time delay between the two chirped lasers and one can collect a 200-cm^{-1} SRS spectrum in 83 μs.[126] In fact, spectral resolution in spectral focusing implementation ($\sim$10–35 cm^{-1}) is mostly lower than a commercial picosecond laser ($\sim$6 cm^{-1}).[117] Parallel SRS imaging can be accomplished by broadband excitation via the combination of ps and fs lasers which is detected by multi-channel PD array either with a lock-in amplifier[41,127] or in a lock-in-free manner.[42,128] To simplify the complexity of common parallel SRS modality, concurrent two-channel SRS imaging at 8 frames per second has been performed utilizing engineered pulse and dual-phase lock-in detection.[39]

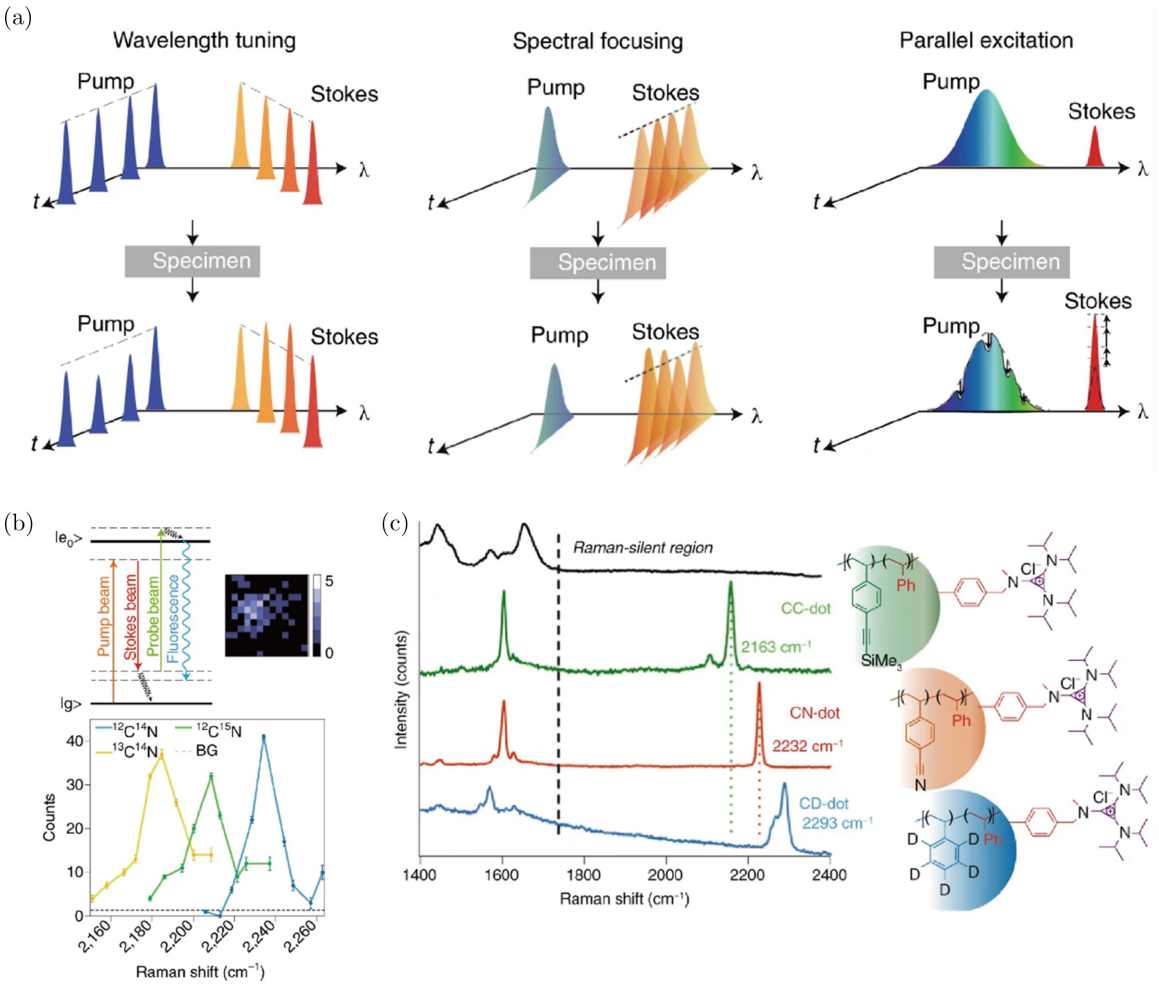

Fig. 2. Technical advances. (a) Multi-mode excitation schemes. Figure adapted from Ref. 116. (b) All-far-field single-molecule vibrational imaging achieved by SREF spectroscopy. Upper: Energy diagram of SREF and a representative single-molecule image of rhodamine 800 (Rh800). Lower: Single-molecule Raman spectrum for Rh800 isotopologs. Figure adapted from Ref. 116. (c) Three-color Raman-active polymer dots by using monomers with small vibrational tags. Figure adapted from Ref. 46.

4.2. *Detection sensitivity*

Note that originally SRS is a label-free technique and is far from the high specificity and sensitivity achieved by fluorescence microscopy. In most cases, the detectability of SRS is in the μM–mM range. Theoretically, the detection sensitivity can be close to the shot noise limit benefiting from MHz modulation and lock-in detection modality.[13] To push the limit of detection sensitivity, different schemes have been developed, including the employment of electronic resonance [Fig. 2(b)] and the development of Raman tags [Fig. 2(c)]. By tuning the absorption of chromophores close to SRS excitation, electronic pre-resonance SRS (epr-SRS) can enhance the Raman scattering cross-section 10^5 times higher and push the detection limit down to sub-μM.[45] Further, stimulated Raman-excited fluorescence (SREF) spectroscopy can achieve single-molecule detection [Fig. 2(b)] by up-converting the SRS-excited vibrational state to electronic fluorescence state followed by fluorescence detection.[32] Otherwise, single-molecule detection can be realized by plasmon-enhanced SRS (PESRS) combining the use of gold nanostructures and de-noising algorithm.[33] Moreover, the sensitivity and specificity can be boosted by the use of Raman tags which mostly locate on the cell Raman-silent region (1800–2700 cm^{-1}). Raman probes contain triple bonds,[62,63,80,85,97,129–133] isotopes,[61,64,65,79,82,134–136] Raman dye palettes[44,45] and Raman-active nanomaterials.[46–49] They exhibit smaller size advantage than fluorescent probes, which makes them highly promising for small-molecule targets. Recently, the usage of squeezed light to break the shot noise limit of SRS has been demonstrated, opening up new possibilities of quantum-enhanced optical imaging.[137–139]

4.3. *Spatial resolution*

As a nonlinear optical imaging technique, SRS has intrinsic sectioning capability similar to two-photon-excited fluorescence, approaching the diffraction-limited resolution. Typically, when using near-infrared excitation wavelength, the lateral resolution is $\sim$300 nm and the axial resolution is $\sim$1 μm. The lateral spatial resolution can be improved to $\sim$130 nm by adopting 450-nm excitation wavelength with a high numerical aperture objective (NA = 1.49).[50] Super-resolution SRS modalities motivated by stimulated emission depletion (STED) fluorescence microscopy have been investigated to exceed the Abbe diffraction limitation, which requires a third laser to suppress SRS signal by saturation/depletion or competition.[51,53,54] Spatial enhancement using doughnut-shaped decoherence beam with high laser power[52] and adopting STED-FM (frequency modulation)-SREF with moderate laser power[57] has been reported. Additionally, inspired by RESOLFT, super-resolution SRS can be realized by devising photoswitchable Raman probes.[58–60]

5. Applications on Biological Cellular Machinery

SRS microscopy has been shown as a powerful video-rate bioimaging platform with spectroscopic information. Here, we highlight its applications on biological cellular machinery, including, but not limited to, mammalian cellular components, metabolisms and microbiology.

5.1. *Imaging cellular components*

The distribution of DNA inside mammalian cells could be mapped based on its intrinsic high-wavenumber C–H fingerprint, followed by real-time recoding of the cell division dynamics and tracking of cell proliferation in drug-induced mouse skin[140] [Figs. 3(a) and 3(b)]. Aside from label-free SRS imaging, alkyne tags offer new perspective to track DNA and RNA dynamics in cell division and proliferation [Figs. 3(c) and 3(d)].[62,131,141] Protein synthesis was visualized by incubating live cells with deuterium-labeled amino acid [Fig. 3(e)].[61] Distribution of lipid droplets and the conversion of retinol to retinoic acids were observed in single live cells.[42] Localization of d_6-desmosterol in NS5A-associated lipid droplets indicated a direct effect on hepatitis C virus replication.[142] Squalene was found to accumulate in the lipid droplets of cholesterol auxotrophic lymphoma cells, which helps in protecting cancer cells from ferroptotic cell death [Fig. 3(f)].[143] Visualization of deuterated fatty acids administered to live cells pinpointed that oleic fatty acids facilitate the conversion of palmitic fatty acid into lipid bodies.[135] Increased unsaturated lipids in ovarian cancer stem cells revealed as a metabolic marker for ovarian cancer, which was mediated by lipid desaturases and regulated by NF-κB survival

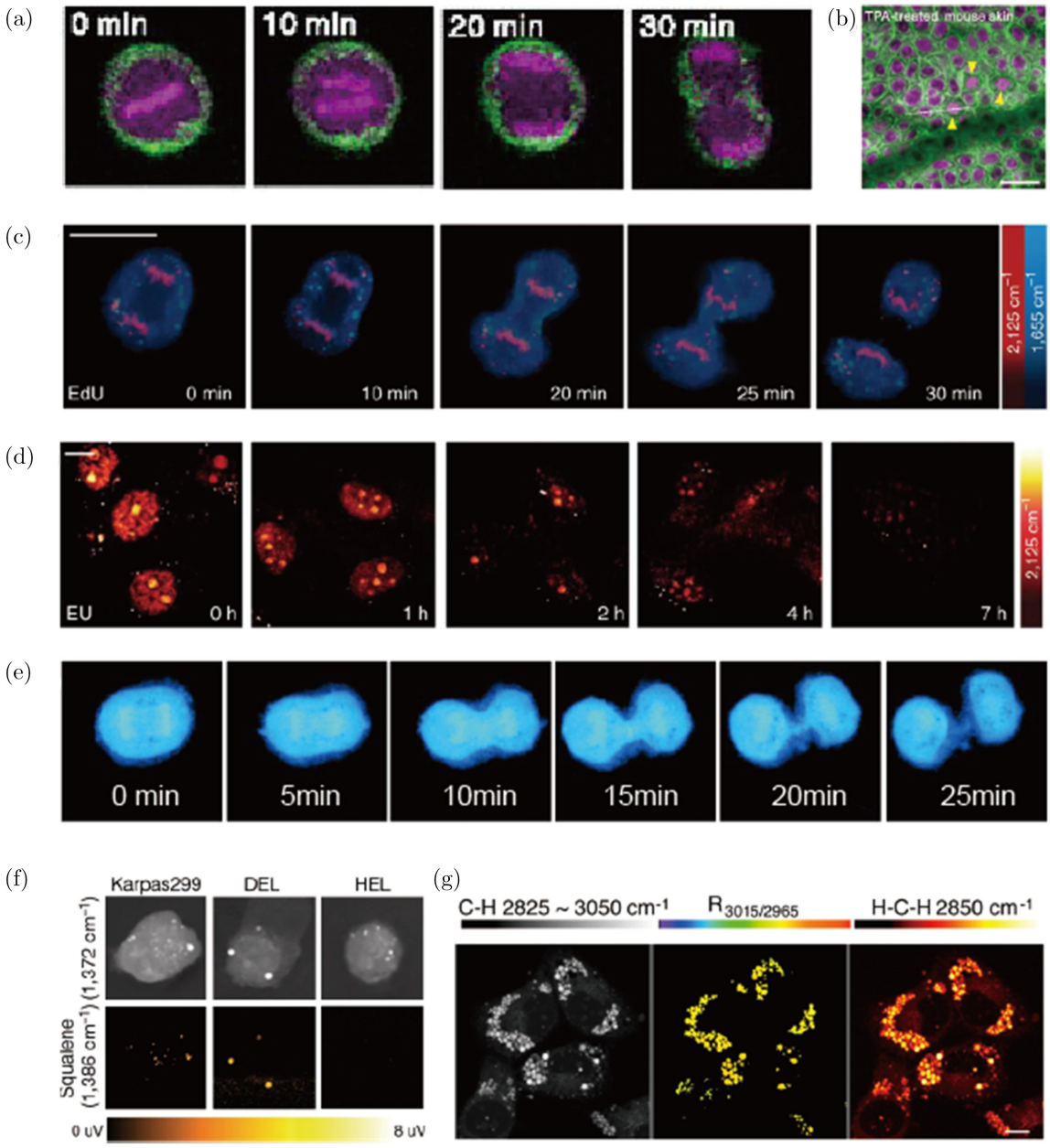

Fig. 3. (Color online) Applications of SRS microscopy in cellular components. (a) Time-lapse label-free imaging of DNA in a HeLa cell undergoing cell division with SRS. Figure adapted from Ref. 140. (b) SRS images of the TPA-treated mouse skin showing increased numbers of the mitotic figures (yellow arrowheads). Figure adapted from Ref. 140. (c) Time-lapse images of a dividing cell incubated with 100-μM EdU. Figure adapted from Ref. 62. (d) Pulse-chase imaging of RNA turnover in HeLa cells incubated with 2-mM EU for 12 h followed by EU-free medium. Figure adapted from Ref. 62. (e) Time-lapse SRS images of a live dividing HeLa cell during a 25-min time course after 20-h incubation with deuterated all-amino-acid medium. Figure adapted from Ref. 61. (f) SRS imaging revealing squalene accumulation in lipid droplets in anaplastic large-cell lymphoma (ALCL) cells. Figure adapted from Ref. 143. (g) Different distributions of neutral lipids in rat hepatic cells McA — cells visualized with hsSRS. R3015/2965 images reveal predominant storage of cholesteryl esters in macrophage cells and triacylglycerols in hepatic cells. Figure adapted from Ref. 145.

pathway.[144] Unsaturated fatty acid was found to prefer lipid storage whereas saturated fatty acid was more likely to exhibit toxicity in cells which incubated with palmitic and arachidonic acids [Fig. 3(g)].[145] Neutral lipid species between individual lipid droplets in a cell was proved to show heterogeneous incorporation by hyperspectral SRS imaging of D38-cholesterol.[65]

5.2. *Dynamics of cell metabolisms*

The dynamics of protein synthesis and degradation inside live cells were captured with the help of deuterated amino acids or ^{13}C-phenalalanine,[79] the aggregation dynamics of huntingtin proteins in live cells was further revealed by two-color pulse-chase imaging [Figs. 4(a)–4(c)].[78] Striking heterogeneity of lipid uptake dynamics in human macrophages was observed when incubated with deuterated palmitic acid.[146] *De novo* lipogenesis in pancreatic cancer cells was visualized directly by tracing the deuterated glucose metabolism dynamics, which occurs faster than in immortalized normal pancreatic epithelial cells [Fig. 4(d)].[136] By tracking the deuterated fatty acids metabolism, saturated fatty acids were reported to form solid-like domains by inducing a phase separation in the endoplasmic reticulum membrane, thus leading to lipotoxicity [Figs. 4(e) and 4(f)].[77] Glucose uptake in tumor cells and neurons was investigated by following the alkyne-labeled glucose (3-OPG).[80] Further, heterogeneous patterns for glucose uptake and incorporation between normal and cancer cells were reported by two-color (^{13}C-3-OPG and d_7-glucose) imaging of glucose metabolism [Fig. 4(g)].[81] Various

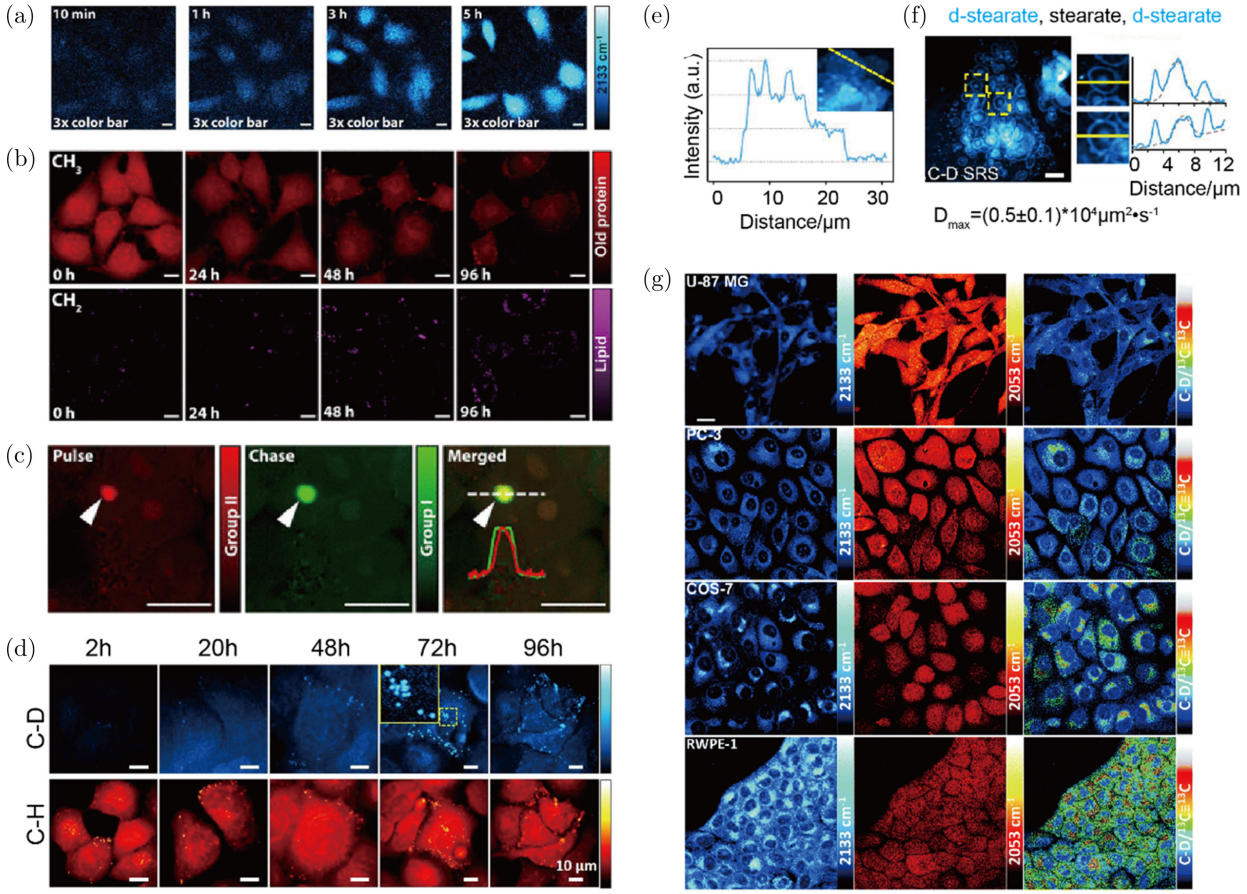

Fig. 4. (Color online) Applications of SRS microscopy on cellular metabolisms. (a) Time-lapse SRS images of protein synthesis dynamics in the same set of live HeLa cells with continuous incubation in optimized deuteration medium. Figure adapted from Ref. 78. (b) Time-dependent SRS imaging of protein degradation in live HeLa cells. Figure adapted from Ref. 78. (c) Two-color pulse-chase imaging of newly synthesized proteins that can be achieved by sequential labeling of group-II and group-I d-amino acids, which shows the dynamic formation process of mutant huntingtin protein aggregate in HeLa cells. Figure adapted from Ref. 78. (d) Monitoring *de novo* lipogenesis in PANC1 cells over time by SRS imaging at C–D and C–H vibrations. Inset of image at 72 h: zoom-in image of marked area showing the donut-shaped newly synthesized LDs. Figure adapted from Ref. 136. (e) Line profiles of C–D SRS image with overlapping layers of palmitate metabolites. Figure adapted from Ref. 77. (f) C–D SRS images of HeLa cell sequentially treated with d-stearate (1 h), stearate (1.5 h) and d-stearate (0.5 h). Intensity profiles (blue) are measured across the yellow lines in regions of interest and fitted with Gaussian function (gray-dashed). The estimated maximum diffusion coefficient (D_{max}) is shown below (mean ± SEM; $n = 21$). Figure adapted from Ref. 77. (g) Two-color glucose metabolism imaging of different cell lines. Figure adapted from Ref. 81.

metabolic activities of newly synthesized DNA, protein, lipids and glycogen were visualized by spectral tracing of d_7-glucose metabolism.[82] Phenyldiyne cholesterol was used to track cholesterol transport from lysosomes to lipid droplets in a cellular model of Niemann–Pick type-C disease with HPβCD treatment.[130] Choline metabolism at single-cell level was traced by deuterated choline.[64]

5.3. *Microbiology*

Rhabduscin was found to locate at the bacterial cell surface where it inhibits phenoloxidases as a potent mechanism to combat host defense.[85] The intracellular metabolite distributions inside *Euglena gracilis* under different culture conditions were video-recorded, where significant metabolic

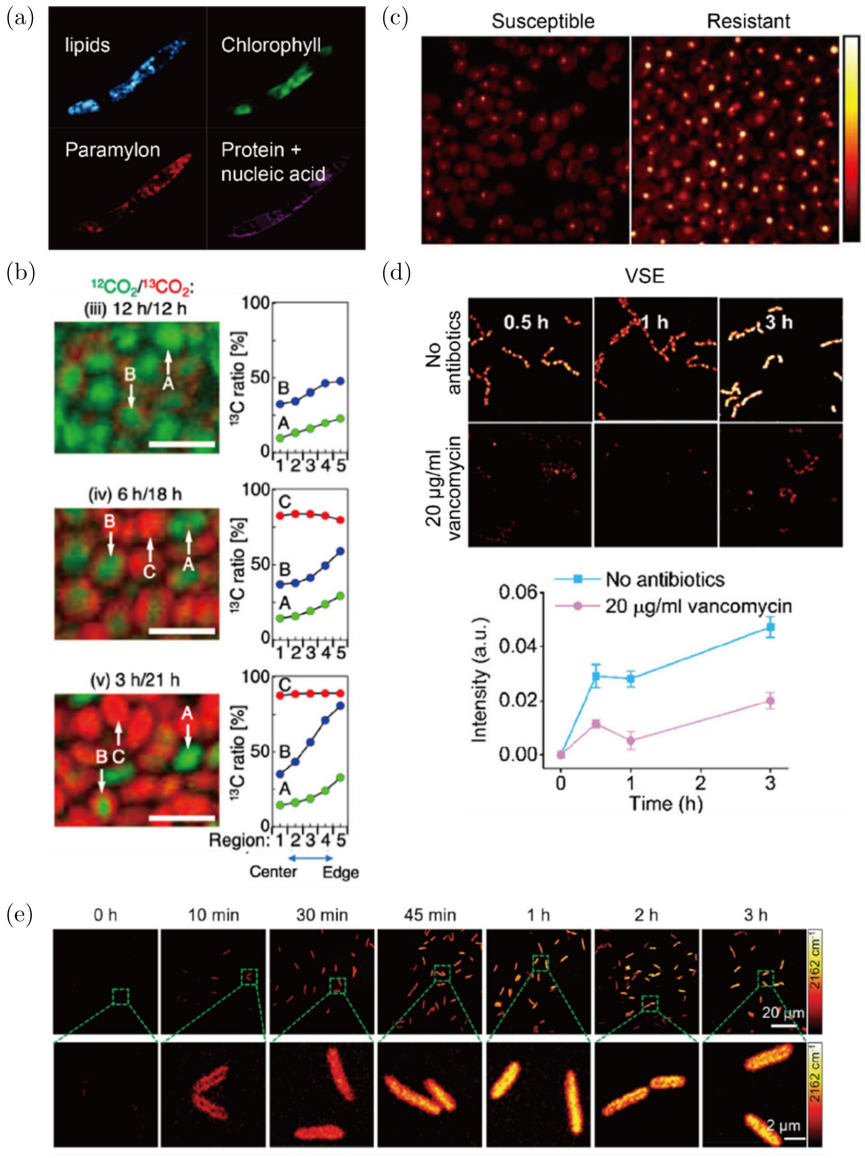

Fig. 5. Applications of SRS microscopy on microbiology. (a) Label-free video-rate SRS imaging showing heterogeneous distribution of metabolites in *E. gracilis* microalgae. Figure adapted from Ref. 37. (b) Left: Magnified SRS images of the extracted paramylon granules that were incubated under different conditions. Representative granules (A: ^{12}C-rich; B: ^{13}C-localized; and C: ^{13}C-rich) are indicated by arrows. Right: Plots of the ^{13}C ratios of the corresponding granules against the five segmented regions. Figure adapted from Ref. 86. (c) C–H frequency (2850-cm^{-1}) SRS images of fluconazole-susceptible and fluconazole-resistant *C. albicans*. Figure adapted from Ref. 88. (d) Upper: Time lapse of C–D component concentration map in vancomycin-susceptible *Enterococci* (VSE) cultivated in glucose-d_7 medium with the presence and absence of 20-μg/mL vancomycin. Lower: Quantitation of C–D component intensity change. Error bars indicate standard deviation (SD, number of cells > 30). Figure adapted from Ref. 89. (E) Time-lapse SRS imaging of *P. aeruginosa* after culture in D_2O-containing medium. Figure adapted from Ref. 90.

heterogeneity with reduced chlorophyll and increased paramylon and lipids was observed under nitrogen-deficiency stress condition [Fig. 5(a)].[37] Further, the biosynthetic process of polysaccharide granules in *Euglena gracilis* was tracked via ^{13}C isotope labeling, giving a hint to elucidate carbon dynamics of storage organelles which could help to enhance the production efficiency of valuable compounds and to screen highly photosynthetic strains [Fig. 5(b)].[86] Considering antibiotic responses, the penetration kinetics of vancomycin into bacterial biofilms was quantitatively monitored by staining with aryl-alkyne.[87] Cellular lipid concentration was presented as a potential marker for antibiotic resistance in *Candida albicans*, enabling rapid detection of antimicrobial susceptibility [Fig. 5(c)].[88] Antibiotic susceptibility testing (AST) at single bacterium level was determined by quantitatively tracking the metabolic uptake of glucose-d_7 in a single live bacterium [Fig. 5(d)].[89] Furthermore, fast AST with the parameter single-cell metabolism inactivation concentration (SC-MIC) in a time less than 2.5 h from colony to results was reported, which probed the D_2O metabolic incorporation into biomass in single bacterium and the metabolic response to antibiotics. Demonstrations of the metabolic activity and susceptibility in urine and whole blood offered the opportunity for rapid single-cell phenotypic AST towards clinical translation [Fig. 5(e)].[90]

6. Conclusion

Since the birth of SRS microscopy, the field has grown tremendously and presented significant contributions to biological and biomedical researches, including cellular biology, cancer biology, microbiology, neurobiology, pharmaceuticals and so on. Although SRS microscopy can be preferable to fluorescence method in many aspects, it has its own shortcomings and challenges. First, the signal intensity of SRS is relatively low, a far cry from fluorescence microscopy. Second, the powers used in SRS are relatively high, which might cause photodamage on biological samples in long-term studies. Third, higher imaging speed is required, especially when balancing with spectroscopic information. In spite of its pitfalls, with further developments SRS is poised to continue paving its way to become a more powerful and robust microscopy technique. Miniatured SRS implementation can be promoted by the development of new fiber laser sources and analysis algorithms, e.g., highly compact, cost-effective and low-noise fiber laser sources and machine learning can help to translate SRS into clinics.[67,71,147] Imaging sensitivity and specificity can be drastically improved by the development of Raman tags with electronic resonance.[32,148] Super-resolution SRS could be promoted by breaking the diffraction limit by a third laser[51,53] or photoswitchable Raman probes.[58–60] By bridging spectral information of SRS with -omics, such as genomics, transcriptomics, proteomics and metabolomics, large-scale cell profiling can be realized. Looking in the foreseeable future, we believe SRS microscopy will continue its vital role in a myriad of biomedical applications.

Acknowledgments

We acknowledge the financial supports from the National Key R&D Program of China (2021YFF0502900), the National Natural Science Foundation of China (61975033), Shanghai Municipal Science and Technology Major Project No. 2018SHZDZX01 and ZJLab.

Conflict of Interest

The authors declare that there are no conflicts of interest relevant to this article.

References

1. R. C. Hooke, *Micrographia: or Some Physiological Descriptions of Minute Bodies made by Magnifying Glasses: With Observations and Inquiries Thereupon*, Royal Society of London, London, England (1665).
2. M. J. Schleiden, Beiträge über phytogenesis, *Müller's Archiv für Anatomie, Physiologie und wissenschaftliche Medicin*, pp. 137–176, Veit et Comp., Leipzig (1838).
3. T. Schwann, "Ueber die analogie in der structur und dem wachsthum der thiere und pflanzen," *Neue Not. Geb. Nat. Heil.* **91**, 33–36 (1838); **103**, 225–229 (1838); **112**, 21–23 (1837).
4. T. Schwann, *Mikroskopische Untersuchungen über die Uebereinstimmung in der Struktur und dem Wachsthum der Thiere und Pflanzen*, Verlag der Sander'schen Buchhandlung (G. E. Reimer), Berlin (1839).

5. J. J. Lister, Roget, "On some properties in achromatic object-glasses applicable to the improvement of the microscope," *Abstracts of the Papers Printed in the Philosophical Transactions of the Royal Society of London*, Vol. 2 (1815–1830), pp. 399–401, The Royal Society, London (1833).
6. T. Araki, "The history of optical microscope," *Mech. Eng. Rev.* **4**(1), 16-00242 (2017).
7. E. Abbe, "Beiträge zur theorie des mikroskops und der mikroskopischen wahrnehmung," *Arch. Mikrosk. Anat.* **9**(1), 413–468 (1873).
8. A. K. M. von Rohr, "Photomicrography with ultraviolet light," *J. R. Microsc. Soc.* **25**, 513 (1905).
9. A. H. Coons, M. H. Kaplan, "Localization of antigen in tissue cells: II: Improvements in a method for the detection of antigen by means of fluorescent antibody," *J. Exp. Med.* **91**(1), 1–13 (1950).
10. M. Minsky, Microscopy apparatus, U.S. Patent No. 3013467 (1961).
11. W. R. Zipfel, R. M. Williams, W. W. Webb, "Nonlinear magic: Multiphoton microscopy in the biosciences," *Nat. Biotechnol.* **21**(11), 1368–1376 (2003).
12. S. H. Yue, M. N. Slipchenko, J. X. Cheng, "Multimodal nonlinear optical microscopy," *Laser Photonics Rev.* **5**(4), 496–512 (2011).
13. W. Min, C. W. Freudiger, S. J. Lu, X. S. Xie, "Coherent nonlinear optical imaging: Beyond fluorescence microscopy," *Annu. Rev. Phys. Chem.* **62**, 507–530 (2011).
14. J. X. Cheng, X. S. Xie, "Vibrational spectroscopic imaging of living systems: An emerging platform for biology and medicine," *Science* **350**(6264), aaa8870 (2015).
15. I. W. Schie, C. Krafft, J. Popp, "Applications of coherent Raman scattering microscopies to clinical and biological studies," *Analyst* **140**(12), 3897–3909 (2015).
16. C. S. Liao, J. X. Cheng, "In situ and in vivo molecular analysis by coherent Raman scattering microscopy," *Annu. Rev. Anal. Chem.* **9**, 69–93 (2016).
17. D. Polli, V. Kumar, C. M. Valensise, M. Marangoni, G. Cerullo, "Broadband coherent Raman scattering microscopy," *Laser Photonics Rev.* **12**(9), 1800020 (2018).
18. M. Manley, "Near-infrared spectroscopy and hyperspectral imaging: non-destructive analysis of biological materials," *Chem. Soc. Rev.* **43**(24), 8200–8214 (2014).
19. R. Bhargava, "Infrared spectroscopic imaging: The next generation," *Appl. Spectrosc.* **66**(10), 1091–1120 (2012).
20. M. Diem, A. Mazur, K. Lenau, J. Schubert, B. Bird, M. Miljkovic, C. Krafft, J. Popp, "Molecular pathology via IR and Raman spectral imaging," *J. Biophotonics* **6**(11–12), 855–886 (2013).
21. M. Diem, A. Ergin, S. Remiszewski, X. Y. Mu, A. Akalin, D. Raz, "Infrared micro-spectroscopy of human tissue: principles and future promises," *Faraday Discuss.* **187**, 9–42 (2016).
22. G. Bellisola, C. Sorio, "Infrared spectroscopy and microscopy in cancer research and diagnosis," *Am. J. Cancer Res.* **2**(1), 1–21 (2012).
23. D. L. Zhang, P. Wang, M. N. Slipchenko, J. X. Cheng, "Fast vibrational imaging of single cells and tissues by stimulated Raman scattering microscopy," *Acc. Chem. Res.* **47**(8), 2282–2290 (2014).
24. M. D. Duncan, J. Reintjes, T. J. Manuccia, "Scanning coherent anti-stokes Raman microscope," *Opt. Lett.* **7**(8), 350–352 (1982).
25. A. Zumbusch, G. R. Holtom, X. S. Xie, "Three-dimensional vibrational imaging by coherent anti-Stokes Raman scattering," *Phys. Rev. Lett.* **82**(20), 4142–4145 (1999).
26. C. W. Freudiger, W. Min, B. G. Saar, S. Lu, G. R. Holtom, C. W. He, J. C. Tsai, J. X. Kang, X. S. Xie, "Label-free biomedical imaging with high sensitivity by stimulated Raman scattering microscopy," *Science* **322**(5909), 1857–1861 (2008).
27. P. Nandakumar, A. Kovalev, A. Volkmer, "Vibrational imaging based on stimulated Raman scattering microscopy," *New J. Phys.* **11**, 033026 (2009).
28. Y. Ozeki, F. Dake, S. Kajiyama, K. Fukui, K. Itoh, "Analysis and experimental assessment of the sensitivity of stimulated Raman scattering microscopy," *Opt. Express* **17**(5), 3651–3658 (2009).
29. W. Min, S. J. Lu, S. S. Chong, R. Roy, G. R. Holtom, X. S. Xie, "Imaging chromophores with undetectable fluorescence by stimulated emission microscopy," *Nature* **461**(7267), 1105–1109 (2009).
30. L. Wei, W. Min, "Electronic preresonance stimulated Raman scattering microscopy," *J. Phys. Chem. Lett.* **9**(15), 4294–4301 (2018).
31. H. Q. Xiong, N. X. Qian, Y. P. Miao, Z. L. Zhao, W. Min, "Stimulated Raman excited fluorescence spectroscopy of visible dyes," *J. Phys. Chem. Lett.* **10**(13), 3563–3570 (2019).
32. H. Q. Xiong, L. X. Shi, L. Wei, Y. H. Shen, R. Long, Z. L. Zhao, W. Min, "Stimulated Raman excited fluorescence spectroscopy and imaging," *Nat. Photonics* **13**(6), 412–417 (2019).
33. C. Zong, R. Premasiri, H. N. Lin, Y. M. Huang, C. Zhang, C. Yang, B. Ren, L. D. Ziegler, J. X. Cheng, "Plasmon-enhanced stimulated Raman scattering microscopy with single-molecule detection sensitivity," *Nat. Commun.* **10**, 5318 (2019).

34. H. Q. Xiong, W. Min, "Combining the best of two worlds: Stimulated Raman excited fluorescence," *J. Chem. Phys.* **153**(21), 210901 (2020).
35. B. G. Saar, C. W. Freudiger, J. Reichman, C. M. Stanley, G. R. Holtom, X. S. Xie, "Video-rate molecular imaging in vivo with stimulated Raman scattering," *Science* **330**(6009), 1368–1370 (2010).
36. Y. Ozeki, W. Umemura, Y. Otsuka, S. Satoh, H. Hashimoto, K. Sumimura, N. Nishizawa, K. Fukui, K. Itoh, "High-speed molecular spectral imaging of tissue with stimulated Raman scattering," *Nat. Photonics* **6**(12), 844–850 (2012).
37. Y. Wakisaka, Y. Suzuki, O. Iwata, A. Nakashima, T. Ito, M. Hirose, R. Domon, M. Sugawara, N. Tsumura, H. Watarai, T. Shimobaba, K. Suzuki, K. Goda, Y. Ozeki, "Probing the metabolic heterogeneity of live *Euglena gracilis* with stimulated Raman scattering microscopy," *Nat. Microbiol.* **1**(10), 16124 (2016).
38. B. Marx, L. Czerwinski, R. Light, M. Somekh, P. Gilch, "Multichannel detectors for femtosecond stimulated Raman microscopy — ideal and real ones," *J. Raman Spectrosc.* **45**(7), 521–527 (2014).
39. R. Y. He, Y. K. Xu, L. L. Zhang, S. H. Ma, X. Wang, D. Ye, M. B. Ji, "Dual-phase stimulated Raman scattering microscopy for real-time two-color imaging," *Optica* **4**(1), 44–47 (2017).
40. D. Fu, F. K. Lu, X. Zhang, C. Freudiger, D. R. Pernik, G. Holtom, X. S. Xie, "Quantitative chemical imaging with multiplex stimulated Raman scattering microscopy," *J. Am. Chem. Soc.* **134**(8), 3623–3626 (2012).
41. K. Seto, Y. Okuda, E. Tokunaga, T. Kobayashi, "Development of a multiplex stimulated Raman microscope for spectral imaging through multichannel lock-in detection," *Rev. Sci. Instrum.* **84**(8), 083705 (2013).
42. C. S. Liao, M. N. Slipchenko, P. Wang, J. J. Li, S. Y. Lee, R. A. Oglesbee, J. X. Cheng, "Microsecond scale vibrational spectroscopic imaging by multiplex stimulated Raman scattering microscopy," *Light, Sci. Appl.* **4**, e265 (2015).
43. C. S. Liao, P. Wang, P. Wang, J. J. Li, H. J. Lee, G. Eakins, J. X. Cheng, "Spectrometer-free vibrational imaging by retrieving stimulated Raman signal from highly scattered photons," *Sci. Adv.* **1**(9), e1500738 (2015).
44. F. H. Hu, C. Zeng, R. Long, Y. P. Miao, L. Wei, Q. Z. Xu, W. Min, "Supermultiplexed optical imaging and barcoding with engineered polyynes," *Nat. Methods* **15**(3), 194–200 (2018).
45. L. Wei, Z. X. Chen, L. X. Shi, R. Long, A. V. Anzalone, L. Y. Zhang, F. H. Hu, R. Yuste, V. W. Cornish, W. Min, "Super-multiplex vibrational imaging," *Nature* **544**(7651), 465–470 (2017).
46. F. H. Hu, S. D. Brucks, T. H. Lambert, L. M. Campos, W. Min, "Stimulated Raman scattering of polymer nanoparticles for multiplexed live-cell imaging," *Chem. Commun.* **53**(46), 6187–6190 (2017).
47. Q. Q. Jin, X. L. Fan, C. M. Chen, L. Huang, J. Wang, X. J. Tang, "Multicolor Raman beads for multiplexed tumor cell and tissue imaging and in vivo tumor spectral detection," *Anal. Chem.* **91**(6), 3784–3789 (2019).
48. Z. L. Zhao, C. Chen, S. X. Wei, H. Q. Xiong, F. H. Hu, Y. P. Miao, T. W. Jin, W. Min, "Ultra-bright Raman dots for multiplexed optical imaging," *Nat. Commun.* **12**(1), 1305 (2021).
49. C. Chen, Z. L. Zhao, N. X. Qian, S. X. Wei, F. H. Hu, W. Min, "Multiplexed live-cell profiling with Raman probes," *Nat. Commun.* **12**(1), 3405 (2021).
50. Y. L. Bi, C. Yang, Y. G. Chen, S. Yan, G. Yang, Y. Z. Wu, G. P. Zhang, P. Wang, "Near-resonance enhanced label-free stimulated Raman scattering microscopy with spatial resolution near 130 nm," *Light, Sci. Appl.* **7**, 81 (2018).
51. D. Kim, D. S. Choi, J. Kwon, S. H. Shim, H. Rhee, M. Cho, "Selective suppression of stimulated Raman scattering with another competing stimulated Raman scattering," *J. Phys. Chem. Lett.* **8**(24), 6118–6123 (2017).
52. W. R. Silva, C. T. Graefe, R. R. Frontiera, "Toward label-free super-resolution microscopy," *ACS Photonics* **3**(1), 79–86 (2016).
53. L. Gong, H. F. Wang, "Suppression of stimulated Raman scattering by an electromagnetically-induced-transparency-like scheme and its application for super-resolution microscopy," *Phys. Rev. A* **92**(2), 023828 (2015).
54. L. Gong, H. Wang, "Breaking the diffraction limit by saturation in stimulated-Raman-scattering microscopy: A theoretical study," *Phys. Rev. A* **90**(1), 013818 (2014).
55. L. Gong, W. Zheng, Y. Ma, Z. W. Huang, "Saturated stimulated-Raman-scattering microscopy for far-field superresolution vibrational imaging," *Phys. Rev. Appl.* **11**(3), 034041 (2019).
56. H. Q. Xiong, N. X. Qian, Z. L. Zhao, L. Y. Shi, Y. P. Miao, W. Min, "Background-free imaging of chemical bonds by a simple and robust frequency-modulated stimulated Raman scattering microscopy," *Opt. Express* **28**(10), 15663–15677 (2020).
57. H. Q. Xiong, N. X. Qian, Y. P. Miao, Z. L. Zhao, C. Chen, W. Min, "Super-resolution vibrational microscopy by stimulated Raman excited fluorescence," *Light, Sci. Appl.* **10**(1), 87 (2021).
58. J. P. Ao, X. F. Fang, X. C. Miao, J. W. Ling, H. Kang, S. Park, C. F. Wu, M. B. Ji, "Switchable

stimulated Raman scattering microscopy with photochromic vibrational probes," *Nat. Commun.* **12**(1), 3089 (2021).
59. D. Lee, C. X. Qian, H. M. Wang, L. Li, K. Miao, J. J. Du, D. M. Shcherbakova, V. V. Verkhusha, L. H. V. Wang, L. Wei, "Toward photoswitchable electronic pre-resonance stimulated Raman probes," *J. Chem. Phys.* **154**(13), 135102 (2021).
60. J. W. Shou, Y. Ozeki, "Photoswitchable stimulated Raman scattering spectroscopy and microscopy," *Opt. Lett.* **46**(9), 2176–2179 (2021).
61. L. Wei, Y. Yu, Y. H. Shen, M. C. Wang, W. Min, "Vibrational imaging of newly synthesized proteins in live cells by stimulated Raman scattering microscopy," *Proc. Natl. Acad. Sci. USA* **110**(28), 11226–11231 (2013).
62. L. Wei, F. H. Hu, Y. H. Shen, Z. X. Chen, Y. Yu, C. C. Lin, M. C. Wang, W. Min, "Live-cell imaging of alkyne-tagged small biomolecules by stimulated Raman scattering," *Nat. Methods* **11**(4), 410–412 (2014).
63. F. H. Hu, M. R. Lamprecht, L. Wei, B. Morrison, W. Min, "Bioorthogonal chemical imaging of metabolic activities in live mammalian hippocampal tissues with stimulated Raman scattering," *Sci. Rep. (UK)* **6**, 39660 (2016).
64. F. H. Hu, L. Wei, C. G. Zheng, Y. H. Shen, W. Min, "Live-cell vibrational imaging of choline metabolites by stimulated Raman scattering coupled with isotope-based metabolic labeling," *Analyst* **139**(10), 2312–2317 (2014).
65. A. Alfonso-Garcia, S. G. Pfisterer, H. Riezman, E. Ikonen, E. O. Potma, "D38-cholesterol as a Raman active probe for imaging intracellular cholesterol storage," *J. Biomed. Opt.* **21**(6), 61003 (2016).
66. C. S. Liao, P. Wang, C. Y. Huang, P. Lin, G. Eakins, R. T. Bentley, R. G. Liang, J. X. Cheng, "*In vivo* and *in situ* spectroscopic imaging by a handheld stimulated Raman scattering microscope," *ACS Photonics* **5**(3), 947–954 (2018).
67. D. A. Orringer, B. Pandian, Y. S. Niknafs, T. C. Hollon, J. Boyle, S. Lewis, M. Garrard, S. L. Hervey-Jumper, H. J. L. Garton, C. O. Maher, J. A. Heth, O. Sagher, D. A. Wilkinson, M. Snuderl, S. Venneti, S. H. Ramkissoon, K. A. McFadden, A. Fisher-Hubbard, A. P. Lieberman, T. D. Johnson, X. S. Xie, J. K. Trautman, C. W. Freudiger, S. Camelo-Piragua, "Rapid intraoperative histology of unprocessed surgical specimens via fibre-laser-based stimulated Raman scattering microscopy," *Nat. Biomed. Eng.* **1**(2), 0027 (2017).
68. J. N. Bentley, M. B. Ji, X. S. Xie, D. A. Orringer, "Real-time image guidance for brain tumor surgery through stimulated Raman scattering microscopy," *Expert Rev. Anticancer Ther.* **14**(4), 359–361 (2014).
69. M. B. Ji, S. Lewis, S. Camelo-Piragua, S. H. Ramkissoon, M. Snuderl, S. Venneti, A. Fisher-Hubbard, M. Garrard, D. Fu, A. C. Wang, J. A. Heth, C. O. Maher, N. Sanai, T. D. Johnson, C. W. Freudiger, O. Sagher, X. S. Xie, D. A. Orringer, "Detection of human brain tumor infiltration with quantitative stimulated Raman scattering microscopy," *Sci. Transl. Med.* **7**(309), 309ra163 (2015).
70. Y. F. Yang, L. C. Chen, M. B. Ji, "Stimulated Raman scattering microscopy for rapid brain tumor histology," *J. Innov. Opt. Health Sci.* **10**(5), 1730010 (2017).
71. T. C. Hollon, B. Pandian, A. R. Adapa, E. Urias, A. V. Save, S. S. S. Khalsa, D. G. Eichberg, R. S. D'Amico, Z. U. Farooq, S. Lewis, P. D. Petridis, T. Marie, A. H. Shah, H. J. L. Garton, C. O. Maher, J. A. Heth, E. L. McKean, S. E. Sullivan, S. L. Hervey-Jumper, P. G. Patil, B. G. Thompson, O. Sagher, G. M. McKhann, R. J. Komotar, M. E. Ivan, M. Snuderl, M. L. Otten, T. D. Johnson, M. B. Sisti, J. N. Bruce, K. M. Muraszko, J. Trautman, C. W. Freudiger, P. Canoll, H. Lee, S. Camelo-Piragua, D. A. Orringer, "Near real-time intraoperative brain tumor diagnosis using stimulated Raman histology and deep neural networks," *Nat. Med.* **26**(1), 52–58 (2020).
72. S. H. Yue, J. J. Li, S. Y. Lee, H. J. Lee, T. Shao, B. Song, L. Cheng, T. A. Masterson, X. Q. Liu, T. L. Ratliff, J. X. Cheng, "Cholesteryl ester accumulation induced by PTEN loss and PI3K/AKT activation underlies human prostate cancer aggressiveness," *Cell Metab.* **19**(3), 393–406 (2014).
73. B. H. Zhang, H. L. Xu, J. Chen, X. X. Zhu, Y. Xue, Y. F. Yang, J. P. Ao, Y. H. Hua, M. B. Ji, "Highly specific and label-free histological identification of microcrystals in fresh human gout tissues with stimulated Raman scattering," *Theranostics* **11**(7), 3074–3088 (2021).
74. K. S. Shin, M. Laohajaratsang, S. Q. Men, B. Figueroa, S. M. Dintzis, D. Fu, "Quantitative chemical imaging of breast calcifications in association with neoplastic processes," *Theranostics* **10**(13), 5865–5878 (2020).
75. Y. F. Yang, Y. L. Yang, Z. J. Liu, L. Guo, S. P. Li, X. J. Sun, Z. M. Shao, M. B. Ji, "Microcalcification-based tumor malignancy evaluation in fresh breast biopsies with hyperspectral stimulated Raman scattering," *Anal. Chem.* **93**(15), 6223–6231 (2021).
76. Z. Liu, W. Su, J. Ao, M. Wang, Q. Jiang, J. He, H. Gao, S. Lei, J. Nie, X. Yan, X. Guo, P. Zhou, H. Hu, M. Ji, "Instant diagnosis of gastroscopic

biopsy via deep-learned single-shot femtosecond stimulated Raman histology," *Nat. Commun.* **13**(1), 4050 (2022).
77. Y. H. Shen, Z. L. Zhao, L. Y. Zhang, L. Y. Shi, S. Shahriar, R. B. Chan, G. Di Paolo, W. Min, "Metabolic activity induces membrane phase separation in endoplasmic reticulum," *Proc. Natl. Acad. Sci. USA* **114**(51), 13394–13399 (2017).
78. L. Wei, Y. H. Shen, F. Xu, F. H. Hu, J. K. Harrington, K. L. Targoff, W. Min, "Imaging complex protein metabolism in live organisms by stimulated Raman scattering microscopy with isotope labeling," *ACS Chem. Biol.* **10**(3), 901–908 (2015).
79. Y. H. Shen, F. Xu, L. Wei, F. H. Hu, W. Min, "Live-cell quantitative imaging of proteome degradation by stimulated Raman scattering," *Angew. Chem., Int. Ed.* **53**(22), 5596–5599 (2014).
80. F. H. Hu, Z. X. Chen, L. Y. Zhang, Y. H. Shen, L. Wei, W. Min, "Vibrational imaging of glucose uptake activity in live cells and tissues by stimulated Raman scattering," *Angew. Chem., Int. Ed.* **54** (34), 9821–9825 (2015).
81. R. Long, L. Y. Zhang, L. Y. Shi, Y. H. Shen, F. H. Hu, C. Zeng, W. Min, "Two-color vibrational imaging of glucose metabolism using stimulated Raman scattering," *Chem. Commun.* **54**(2), 152–155 (2018).
82. L. Y. Zhang, L. Y. Shi, Y. H. Shen, Y. P. Miao, M. Wei, N. X. Qian, Y. N. Liu, W. Min, "Spectral tracing of deuterium for imaging glucose metabolism," *Nat. Biomed. Eng.* **3**(5), 402–413 (2019).
83. F. Tian, W. L. Yang, D. A. Mordes, J. Y. Wang, J. S. Salameh, J. Mok, J. Chew, A. Sharma, E. Leno-Duran, S. Suzuki-Uematsu, N. Suzuki, S. S. Han, F. K. Lu, M. B. A. Ji, R. Zhang, Y. Liu, J. Strominger, N. A. Shneider, L. Petrucelli, X. S. Xie, K. Eggan, "Monitoring peripheral nerve degeneration in ALS by label-free stimulated Raman scattering imaging," *Nat. Commun.* **7**, 13283 (2016).
84. M. B. Ji, M. Arbel, L. L. Zhang, C. W. Freudiger, S. S. Hou, D. D. Lin, X. J. Yang, B. J. Bacskai, X. S. Xie, "Label-free imaging of amyloid plaques in Alzheimer's disease with stimulated Raman scattering microscopy," *Sci. Adv.* **4**(11), 31 (2022).
85. J. M. Crawford, C. Portmann, X. Zhang, M. B. J. Roeffaers, J. Clardy, "Small molecule perimeter defense in entomopathogenic bacteria," *Proc. Natl. Acad. Sci USA* **109**(27), 10821–10826 (2012).
86. Y. Yonamine, T. Asai, Y. Suzuki, T. Ito, Y. Ozeki, Y. Hoshino, "Probing the biogenesis of polysaccharide granules in algal cells at sub-organellar resolution via Raman microscopy with stable isotope labeling," *Anal. Chem.* **93**(50), 16796–16803 (2021).
87. K. Bae, W. Zheng, Y. Ma, Z. W. Huang, "Real-time monitoring of pharmacokinetics of antibiotics in biofilms with Raman-tagged hyperspectral stimulated Raman scattering microscopy," *Theranostics* **9**(5), 1348–1357 (2019).
88. C. W. Karanja, W. L. Hong, W. Younis, H. E. Eldesouky, M. N. Seleem, J. X. Cheng, "Stimulated Raman imaging reveals aberrant lipogenesis as a metabolic marker for azole-resistant *Candida albicans*," *Anal. Chem.* **89**(18), 9822–9829 (2017).
89. W. L. Hong, C. W. Karanja, N. S. Abutaleb, W. Younis, X. Y. Zhang, M. N. Seleem, J. X. Cheng, "Antibiotic susceptibility determination within one cell cycle at single-bacterium level by stimulated Raman metabolic imaging," *Anal. Chem.* **90**(6), 3737–3743 (2018).
90. M. Zhang, W. L. Hong, N. S. Abutaleb, J. J. Li, P. T. Dong, C. Zong, P. Wang, M. N. Seleem, J. X. Cheng, "Rapid determination of antimicrobial susceptibility by stimulated Raman scattering imaging of D_2O metabolic incorporation in a single bacterium," *Adv. Sci.* **7**(19), 2001452 (2020).
91. W. J. Tipping, M. Lee, A. Serrels, V. G. Brunton, A. N. Hulme, "Stimulated Raman scattering microscopy: An emerging tool for drug discovery," *Chem. Soc. Rev.* **45**(8), 2075–2089 (2016).
92. M. N. Slipchenko, H. T. Chen, D. R. Ely, Y. Jung, M. T. Carvajal, J. X. Cheng, "Vibrational imaging of tablets by epi-detected stimulated Raman scattering microscopy," *Analyst* **135**(10), 2613–2619 (2010).
93. A. T. Francis, T. T. Nguyen, M. S. Lamm, R. Teller, S. P. Forster, W. Xu, T. Rhodes, R. L. Smith, J. Kuiper, Y. C. Su, D. Fu, "In situ stimulated Raman scattering (SRS) microscopy study of the dissolution of sustained-release implant formulation," *Mol. Pharmaceut.* **15**(12), 5793–5801 (2018).
94. D. Fu, J. Zhou, W. S. Zhu, P. W. Manley, Y. K. Wang, T. Hood, A. Wylie, X. S. Xie, "Imaging the intracellular distribution of tyrosine kinase inhibitors in living cells with quantitative hyperspectral stimulated Raman scattering," *Nat. Chem.* **6**(7), 615–623 (2014).
95. W. J. Tipping, M. Lee, A. Serrels, V. G. Brunton, A. N. Hulme, "Imaging drug uptake by bioorthogonal stimulated Raman scattering microscopy," *Chem. Sci.* **8**(8), 5606–5615 (2017).
96. E. R. Seidel, Y. P. Miao, L. Porterfield, W. L. Cai, X. J. Zhu, S. O. O. Kim, F. H. Hu, S. T. L. N. Bhattarai, W. Min, W. J. Zhang, "Structure-activity-distribution relationship study of anti-cancer antimycin-type depsipeptides," *Chem. Commun.* **55**(63), 9379–9382 (2019).

97. M. M. Gaschler, F. H. Hu, H. Z. Feng, A. Linkermann, W. Min, B. R. Stockwell, "Determination of the subcellular localization and mechanism of action of ferrostatins in suppressing ferroptosis," *ACS Chem. Biol.* **13**(4), 1013–1020 (2018).
98. Q. Cheng, L. Wei, Z. Liu, N. Ni, Z. Sang, B. Zhu, W. H. Xu, M. J. Chen, Y. P. Miao, L. Q. Chen, W. Min, Y. Yang, "Operando and three-dimensional visualization of anion depletion and lithium growth by stimulated Raman scattering microscopy," *Nat. Commun.* **9**, 2942 (2018).
99. J. W. Ling, X. C. Miao, Y. Y. Sun, Y. Q. Feng, L. W. Zhang, Z. Z. Sun, M. B. Ji, "Vibrational imaging and quantification of two-dimensional hexagonal boron nitride with stimulated Raman scattering," *ACS Nano* **13**(12), 14033–14040 (2019).
100. J. P. Ao, Y. Q. Feng, S. M. Wu, T. Wang, J. W. Ling, L. W. Zhang, M. B. Ji, "Rapid, 3D chemical profiling of individual atmospheric aerosols with stimulated Raman scattering microscopy," *Small Methods* **4**(2), 1900600 (2020).
101. H. Z. Li, Y. Cheng, H. J. Tang, Y. L. Bi, Y. G. Chen, G. Yang, S. J. Guo, S. D. Tian, J. S. Liao, X. H. Lv, S. Q. Zeng, M. Q. Zhu, C. J. Xu, J. X. Cheng, P. Wang, "Imaging chemical kinetics of radical polymerization with an ultrafast coherent Raman microscope," *Adv. Sci.* **7**(10), 1903644 (2020).
102. L. Zada, H. A. Leslie, A. D. Vethaak, G. H. Tinnevelt, J. J. Jansen, J. F. de Boer, F. Ariese, "Fast microplastics identification with stimulated Raman scattering microscopy," *J. Raman Spectrosc.* **49**(7), 1136–1144 (2018).
103. M. A. Houle, R. C. Burruss, A. Ridsdale, D. J. Moffatt, F. Legare, A. Stolow, "Rapid 3D chemical-specific imaging of minerals using stimulated Raman scattering microscopy," *J. Raman Spectrosc.* **48**(5), 726–735 (2017).
104. C. V. Raman, K. S. Krishnan, "A new type of secondary radiation," *Nature* **121**, 501–502 (1928).
105. H. Rigneault, P. Berto, "Tutorial: Coherent Raman light matter interaction processes," *APL Photonics* **3**(9), 091101 (2018).
106. M. Schmitt, T. Mayerhöfer, J. Popp, I. Kleppe, K. Weisshart, Light–matter interaction: Part 1: Basics and techniques, *Handbook of Biophotonics*, 1st Edition, J. Popp, V. V. Tuchin, A. Chiou, S. H. Heinemann, Eds., Vol. 1, pp. 87–261, Wiley-VCH Verlag GmbH & Co. KGaA, Berlin (2012).
107. G. W. Auner, S. K. Koya, C. H. Huang, B. Broadbent, M. Trexler, Z. Auner, A. Elias, K. C. Mehne, M. A. Brusatori, "Applications of Raman spectroscopy in cancer diagnosis," *Cancer Metastasis Rev.* **37**(4), 691–717 (2018).
108. C. Krafft, B. Dietzek, M. Schmitt, J. Popp, "Raman and coherent anti-Stokes Raman scattering microspectroscopy for biomedical applications," *J. Biomed. Opt.* **17**(4), 040801 (2012).
109. K. Kong, C. Kendall, N. Stone, I. Notingher, "Raman spectroscopy for medical diagnostics — From in-vitro biofluid assays to in-vivo cancer detection," *Adv. Drug Deliv. Rev.* **89**, 121–134 (2015).
110. C. Krafft, M. Schmitt, I. W. Schie, D. Cialla-May, C. Matthaus, T. Bocklitz, J. Popp, "Label-free molecular imaging of biological cells and tissues by linear and nonlinear Raman spectroscopic approaches," *Angew. Chem., Int. Ed.* **56**(16), 4392–4430 (2017).
111. R. C. Prince, R. R. Frontiera, E. O. Potma, "Stimulated Raman scattering: From bulk to nano," *Chem. Rev.* **117**(7), 5070–5094 (2017).
112. C. L. Evans, X. S. Xie, "Coherent anti-Stokes Raman scattering microscopy: Chemical imaging for biology and medicine," *Annu. Rev. Anal. Chem.* **1**, 883–909 (2008).
113. J. Chan, S. Fore, S. Wachsman-Hogiu, T. Huser, "Raman spectroscopy and microscopy of individual cells and cellular components," *Laser Photonics Rev.* **2**(5), 325–349 (2008).
114. C. Krafft, J. Popp, "The many facets of Raman spectroscopy for biomedical analysis," *Anal. Bioanal. Chem.* **407**(3), 699–717 (2015).
115. C. Krafft, B. Dietzek, J. Popp, "Raman and CARS microspectroscopy of cells and tissues," *Analyst* **134**(6), 1046–1057 (2009).
116. F. H. Hu, L. X. Shi, W. Min, "Biological imaging of chemical bonds by stimulated Raman scattering microscopy," *Nat. Methods* **16**(9), 830–842 (2019).
117. A. H. Hill, D. Fu, "Cellular imaging using stimulated Raman scattering microscopy," *Anal. Chem.* **91**(15), 9333–9342 (2019).
118. L. J. Kong, M. B. Ji, G. R. Holtom, D. Fu, C. W. Freudiger, X. S. Xie, "Multicolor stimulated Raman scattering microscopy with a rapidly tunable optical parametric oscillator," *Opt. Lett.* **38**(2), 145–147 (2013).
119. J. L. Suhalim, C. Y. Chung, M. B. Lilledahl, R. S. Lim, M. Levi, B. J. Tromberg, E. O. Potma, "Characterization of cholesterol crystals in atherosclerotic plaques using stimulated Raman scattering and second-harmonic generation microscopy," *Biophys. J.* **102**(8), 1988–1995 (2012).
120. C. W. Freudiger, W. Min, G. R. Holtom, B. W. Xu, M. Dantus, X. S. Xie, "Highly specific label-free molecular imaging with spectrally tailored excitation-stimulated Raman scattering (STE-SRS) microscopy," *Nat. Photonics* **5**(2), 103–109 (2011).

121. D. L. Zhang, P. Wang, M. N. Slipchenko, D. Ben-Amotz, A. M. Weiner, J. X. Cheng, "Quantitative vibrational imaging by hyperspectral stimulated Raman scattering microscopy and multivariate curve resolution analysis," *Anal. Chem.* **85**(1), 98–106 (2013).
122. E. R. Andresen, P. Berto, H. Rigneault, "Stimulated Raman scattering microscopy by spectral focusing and fiber-generated soliton as Stokes pulse," *Opt. Lett.* **36**(13), 2387–2389 (2011).
123. D. Fu, G. Holtom, C. Freudiger, X. Zhang, X. S. Xie, "Hyperspectral imaging with stimulated Raman scattering by chirped femtosecond lasers," *J. Phys. Chem. B* **117**(16), 4634–4640 (2013).
124. R. Y. He, Z. P. Liu, Y. K. Xu, W. Huang, H. Ma, M. B. Ji, "Stimulated Raman scattering microscopy and spectroscopy with a rapid scanning optical delay line," *Opt. Lett.* **42**(4), 659–662 (2017).
125. M. S. Alshaykh, C. S. Liao, O. E. Sandoval, G. Gitzinger, N. Forget, D. E. Leaird, J. X. Cheng, A. M. Weiner, "High-speed stimulated hyperspectral Raman imaging using rapid acousto-optic delay lines," *Opt. Lett.* **42**(8), 1548–1551 (2017).
126. C. S. Liao, K. C. Huang, W. L. Hong, A. J. Chen, C. Karanja, P. Wang, G. Eakins, J. X. Cheng, "Stimulated Raman spectroscopic imaging by microsecond delay-line tuning," *Optica* **3**(12), 1377–1380 (2016).
127. F. K. Lu, M. B. Ji, D. Fu, X. H. Ni, C. W. Freudiger, G. Holtom, X. S. N. Xie, "Multicolor stimulated Raman scattering microscopy," *Mol. Phys.* **110**(15–16), 1927–1932 (2012).
128. C. Zhang, K. C. Huang, B. Rajwa, J. J. Li, S. Q. Yang, H. N. Lin, C. S. Liao, G. Eakins, S. H. Kuang, V. Patsekin, J. P. Robinson, J. X. Cheng, "Stimulated Raman scattering flow cytometry for label-free single-particle analysis," *Optica* **4**(1), 103–109 (2017).
129. S. L. Hong, T. Chen, Y. T. Zhu, A. Li, Y. Y. Huang, X. Chen, "Live-cell stimulated Raman scattering imaging of alkyne-tagged biomolecules," *Angew. Chem., Int. Ed.* **53**(23), 5827–5831 (2014).
130. H. J. Lee, W. D. Zhang, D. L. Zhang, Y. Yang, B. Liu, E. L. Barker, K. K. Buhman, L. V. Slipchenko, M. J. Dai, J. X. Cheng, "Assessing cholesterol storage in live cells and *C. elegans* by stimulated Raman scattering imaging of phenyldiyne cholesterol, *Sci. Rep. (UK)* **5**, 7930 (2015).
131. Z. X. Chen, D. W. Paley, L. Wei, A. L. Weisman, R. A. Friesner, C. Nuckolls, W. Min, "Multicolor live-cell chemical imaging by isotopically edited alkyne vibrational palette," *J. Am. Chem. Soc.* **136**(22), 8027–8033 (2014).
132. J. C. Mansfield, G. R. Littlejohn, M. P. Seymour, R. J. Lind, S. Perfect, J. Moger, "Label-free chemically specific imaging in planta with stimulated Raman scattering microscopy," *Anal. Chem.* **85**(10), 5055–5063 (2013).
133. W. Zhu, E. L. Cai, H. Z. Li, P. Wang, A. G. Shen, J. Popp, J. M. Hu, "Precise encoding of triple-bond Raman scattering of single polymer nanoparticles for multiplexed imaging application," *Angew. Chem., Int. Ed.* **60**(40), 21846–21852 (2021).
134. B. G. Saar, L. R. Contreras-Rojas, X. S. Xie, R. H. Guy, "Imaging drug delivery to skin with stimulated Raman scattering microscopy," *Mol. Pharmaceut.* **8**(3), 969–975 (2011).
135. D. Zhang, M. N. Sipchenko, J. X. Cheng, "Highly sensitive vibrational imaging by femtosecond pulse stimulated Raman loss," *J. Phys. Chem. Lett.* **2**(11), 1248–1253 (2011).
136. J. J. Li, J. X. Cheng, "Direct visualization of *de novo* lipogenesis in single living cells," *Sci. Rep. (UK)* **4**, 6807 (2014).
137. C. A. Casacio, L. S. Madsen, A. Terrasson, M. Waleed, K. Barnscheidt, B. Hage, M. A. Taylor, W. P. Bowen, "Quantum-enhanced nonlinear microscopy," *Nature* **594**(7862), 201–206 (2021).
138. Z. C. Xu, K. Oguchi, Y. Taguchi, Y. Sano, Y. Miyawaki, D. Cheon, K. Katoh, Y. Ozeki, "Stimulated Raman scattering spectroscopy with quantum-enhanced balanced detection," *Opt. Express* **30**(11), 18589–18598 (2022).
139. R. B. de Andrade, H. Kerdoncuff, K. Berg-Sorensen, T. Gehring, M. Lassen, U. L. Andersen, "Quantum-enhanced continuous-wave stimulated Raman scattering spectroscopy," *Optica* **7**(5), 470–475 (2020).
140. F. K. Lu, S. Basu, V. Igras, M. P. Hoang, M. B. Ji, D. Fu, G. R. Holtom, V. A. Neel, C. W. Freudiger, D. E. Fisher, X. S. Xie, "Label-free DNA imaging in vivo with stimulated Raman scattering microscopy," *Proc. Natl. Acad. Sci. USA* **112**(37), 11624–11629 (2015).
141. H. Yamakoshi, K. Dodo, M. Okada, J. Ando, A. Palonpon, K. Fujita, S. Kawata, M. Sodeoka, "Imaging of EdU, an alkyne-tagged cell proliferation probe, by Raman microscopy," *J. Am. Chem. Soc.* **133**(16), 6102–6105 (2011).
142. V. A. Villareal, D. Fu, D. A. Costello, X. S. Xie, P. L. Yang, "Hepatitis C virus selectively alters the intracellular localization of desmosterol," *ACS Chem. Biol.* **11**(7), 1827–1833 (2016).
143. J. Garcia-Bermudez, L. Baudrier, E. C. Bayraktar, Y. H. Shen, K. La, R. Guarecuco, B. Yucel, D. Fiore, B. Tavora, E. Freinkman, S. H. Chan, C. Lewis, W. Min, G. Inghirami, D. M. Sabatini, K. Birsoy, "Squalene accumulation in cholesterol

auxotrophic lymphomas prevents oxidative cell death," *Nature* **567**(7746), 118–122 (2019).

144. J. J. Li, S. Condello, J. Thomes-Pepin, X. X. Ma, Y. Xia, T. D. Hurley, D. Matei, J. X. Cheng, "Lipid desaturation is a metabolic marker and therapeutic target of ovarian cancer stem cells," *Cell Stem Cell* **20**(3), 303–314 (2017).
145. D. Fu, Y. Yu, A. Folick, E. Currie, R. V. Farese, T. H. Tsai, X. S. Xie, M. C. Wang, "In vivo metabolic fingerprinting of neutral lipids with hyperspectral stimulated Raman scattering microscopy," *J. Am. Chem. Soc.* **136**(24), 8820–8828 (2014).
146. C. Stiebing, T. Meyer, I. Rimke, C. Matthus, M. Schmitt, S. Lorkowski, J. Popp, "Real-time Raman and SRS imaging of living human macrophages reveals cell-to-cell heterogeneity and dynamics of lipid uptake," *J. Biophotonics* **10**(9), 1217–1226 (2017).
147. T. C. Hollon, S. Lewis, B. Pandian, Y. S. Niknafs, M. R. Garrard, H. Garton, C. O. Maher, K. McFadden, M. Snuderl, A. P. Lieberman, K. Muraszko, S. Camelo-Piragua, D. A. Orringer, "Rapid intraoperative diagnosis of pediatric brain tumors using stimulated Raman histology," *Cancer Res.* **78**(1), 278–289 (2018).
148. L. X. Shi, F. H. Hu, W. Min, "Optical mapping of biological water in single live cells by stimulated Raman excited fluorescence microscopy," *Nat. Commun.* **10**, 4764 (2019).